

Thermodynamic versus statistical local equilibrium in nonequilibrium fluids

J.J. del Pozo,^{*} P.L. Garrido,[†] and P.I. Hurtado[‡]

Institute Carlos I for Theoretical and Computational Physics,

and Departamento de Electromagnetismo y Física de la Materia, Universidad de Granada, 18071 Granada, Spain

(Dated: December 6, 2024)

We use extensive computer simulations to probe local thermodynamic equilibrium (LTE) in a quintessential model fluid, the two-dimensional hard-disks system. We show that macroscopic LTE is a very strong property, even in the presence of important finite size effects, revealing a remarkable bulk-boundary decoupling phenomenon in fluids out of equilibrium. These properties allow us to measure the hard disks equation of state in simulations far from equilibrium, with a stunning accuracy comparable to the best equilibrium simulations. Subtle corrections to LTE are found in the fluctuations of the total energy which strongly point out to the nonlocality of the nonequilibrium potential governing the fluid's macroscopic behavior out of equilibrium.

PACS numbers: 05.40.-a, 05.70.Ln, 74.40.Gh, 65.20.-w

Nonequilibrium phenomena characterize the physics of many natural systems, and their understanding remains as a major challenge of modern theoretical physics. Out of equilibrium, dynamics and statistics are so intimately knotted that no general bottom-up approach exists yet capable of predicting nonequilibrium macroscopic behavior in terms of microscopic physics, even in the simplest situation of a nonequilibrium steady state (NESS) [1–7]. In contrast with equilibrium, the microscopic probability measure associated to a NESS (or mNESS hereafter) is a complex object, often defined on a fractal support or strange attractor, and is utterly sensitive to microscopic details as the modeling of boundary reservoirs (e.g., deterministic vs stochastic) [2, 8–10]. Moreover, the connection between mNESSs and a nonequilibrium analog of thermodynamic potentials is still murky at best. On the other hand, we do know that essentially different mNESSs (resulting e.g. from different modelings of boundary baths) describe equally well what seems to be the same macroscopic NESS (or MNESS in short), defined in terms of a few macroscopically smooth fields [11]. Key for this sort of nonequilibrium ensemble equivalence (which can be formally stated via the *chaotic hypothesis* of Gallavotti and Cohen [10]) is the notion of local thermodynamic equilibrium (LTE) [2, 12], i.e. the fact that an interacting nonequilibrium system reaches *locally* an equilibrium-like state defined by e.g. a local temperature, density and velocity (the first two related locally via standard thermodynamics), which are roughly constant across molecular scales but change smoothly at much larger macroscopic scales, where their evolution is governed by hydrodynamic equations. LTE plays an important role in physics, being at the heart of many successful theories, from the classical hydrodynamics [13] or nonequilibrium thermodynamics [14] to recent macroscopic fluctuation theory (MFT) [4–7]. The latter studies dynamic fluctuations of macroscopic observables arbitrary far from equilibrium, and offers explicit predictions for the large deviation functions (LDFs) controlling the

statistics of these fluctuations [15]. These LDFs play in nonequilibrium a role akin to the free energy (or entropy) in equilibrium systems, establishing MFT as an alternative pathway to derive thermodynamic-like potentials out of equilibrium, bypassing the complexities associated to mNESSs and their sensitivity to microscopic details [4, 5]. The LDFs so obtained exhibit the hallmarks of nonequilibrium behavior, e.g. they are typically nonlocal (or equivalently nonadditive) [16] in stark contrast with equilibrium phenomenology. Such nonlocality emerges from tiny, $\mathcal{O}(N^{-1})$ corrections to LTE which spread over macroscopic regions of size $\mathcal{O}(N)$, with N the number of particles in the system of interest [16]. This shows that LTE is a subtle property: while corrections to LTE vanish locally in the $N \rightarrow \infty$ limit, they have a fundamental impact on nonequilibrium LDFs in the form of nonlocality, which in turn gives rise to the ubiquitous long-range correlations which characterize nonequilibrium fluids [4, 17, 18].

These fundamental insights about LTE and its role out of equilibrium are coming forth from the study of a few oversimplified stochastic models of transport [4–7, 16]. The question remains however as to whether the emerging picture endures in more realistic systems: Does LTE hold at the macroscopic level in fluids far from equilibrium? Can we measure corrections to LTE at the microscopic or fluctuating level? Are these corrections the fingerprints of nonlocality? Here we answer these questions for a quintessential model of a nonequilibrium fluid, the two-dimensional hard-disks system under a temperature gradient [19]. In particular, we show that macroscopic LTE (MLTE) is a very strong property even in the presence of important finite size effects, revealing a striking decoupling between the bulk fluid, which behaves macroscopically, and two boundary layers which sum up all sorts of spurious finite-size and boundary corrections to renormalize the effective boundary conditions on the remaining bulk. This bulk-boundary decoupling phenomenon, together with the robustness of the

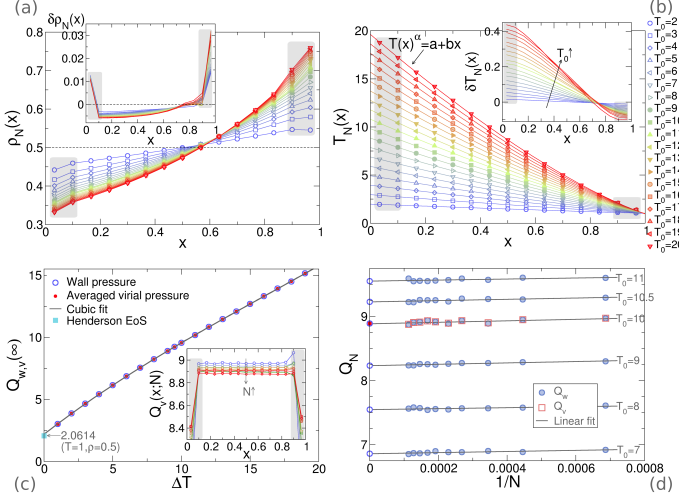


FIG. 1. (Color online) (a) Density profiles for $N = 8838$, $\eta = 0.5$ and varying $T_0 \in [2, 20]$. Shaded areas correspond to boundary layers. Inset: Finite size effects as captured by $\delta\rho_N(x) \equiv \rho_{N_{\max}}(x) - \rho_{N_{\min}}(x)$, with $N_{\max} = 8838$ and $N_{\min} = 1456$, for different gradients. (b) Temperature profiles for the same conditions, and finite-size effects (inset). Lines are nonlinear fits of the form $T(x)^\alpha = ax + b$ [22, 23]. (c) Virial and wall reduced pressures as a function of ΔT for $\eta = 0.5$ in the $N \rightarrow \infty$ limit, and cubic fit. In both cases finite-size data scale linearly with N^{-1} , see panel (d). The inset in (c) shows virial pressure profiles for different N , $\eta = 0.5$ and $\Delta T = 10$, which are constant in the bulk.

MLTE property, allows to measure with stunning accuracy the *equilibrium* equation of state (EoS) of hard disks in nonequilibrium simulations, even across the controversial hexatic and solid phases [20]. To search for corrections to LTE, we study the moments of the velocity field and the total energy. While the former do not exhibit corrections to LTE, the fluctuations of the total energy do pick up these small corrections, the essential difference coming from the nonlocal character of the higher-order moments of the total energy. This suggests that corrections to LTE are indeed linked to the nonlocality of the nonequilibrium fluid.

We hence consider a system of $N \in [1456, 8838]$ hard disks of radius ℓ in a two-dimensional box of unit size $L = 1$, with stochastic thermal walls [21] at $x = 0$, L at temperatures $T_0 \in [2, 20]$ and $T_L = 1$, respectively, and periodic boundary conditions along the y -direction. The disks radius is defined as $\ell = \sqrt{\eta/N\pi}$, with $\eta = \pi\ell^2 N/L^2 \in [0.05, 0.725]$ the global packing fraction, so that we can approach the $N \rightarrow \infty$ limit at fixed η and temperature gradient $\Delta T \equiv |T_L - T_0|/L$. We divided the system into 15 virtual cells along the gradient direction, and measured locally a number of relevant observables including the local average kinetic energy, virial pressure, packing fraction, etc., as well as the heat current flowing through the thermal baths and the pressure exerted on the walls. Time averages were performed with measurements every 10 time units for a total time of $10^6 - 10^7$

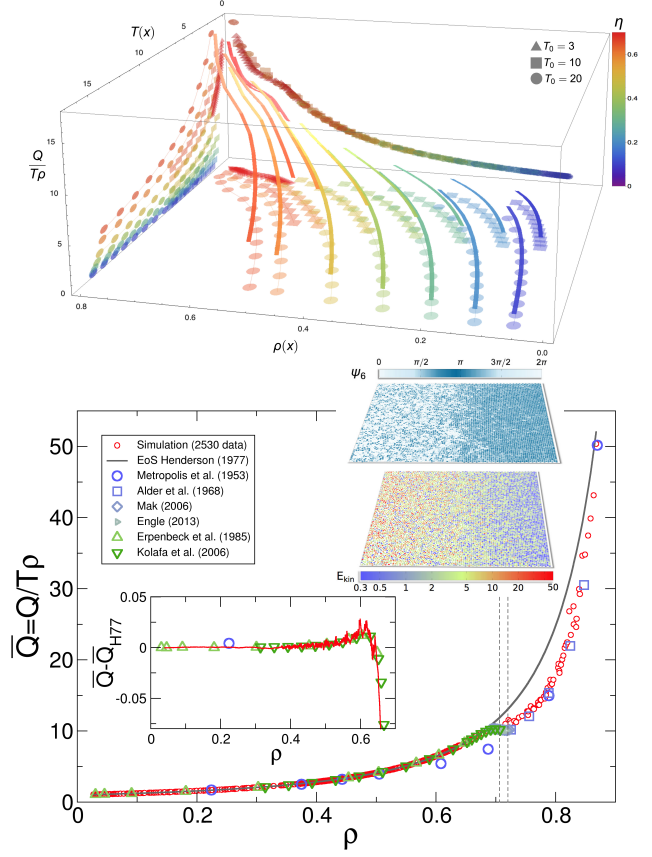


FIG. 2. (Color online) Top: $\bar{Q}_N \equiv Q_N/[T_N(x)\rho_N(x)]$ as a function of $T_N(x)$ and $\rho_N(x)$ measured for $N = 2900$ and varying η and T_0 . Bottom: \bar{Q}_N vs $\rho_N(x)$ measured for $\eta = 0.5$, $N \in [1456, 8838]$ and $T_0 \in [2, 20]$, as well as for $\eta \in [0.05, 0.65]$, $N = 2900$ and $T_0 = 10, 20$, summing up a total of 2530 data points. For comparison, data from previous equilibrium simulations in literature are shown, together with the Henderson EoS approximation (line). The bottom inset shows a detailed comparison of a running average of our data with equilibrium results after subtracting the leading Henderson behavior. Top inset: Snapshot of a typical configuration with $N = 7838$, $\eta = 0.7$ and $T_0 = 10$ and two color codes representing respectively the local hexatic order (top) and the kinetic energy (bottom). Fluid and solid phases coexist for such high η under a temperature gradient.

(our time unit was set to one collision per particle on average), after a relaxation time of 10^3 which was sufficient to reach the steady state. Small corrections ($\sim 0.1\%$) due to the spatial discretization of profiles are explicitly taken into account and subtracted (see Appendix A), and statistical errors in data averages (at a 99.7% confidence level) are always plotted.

Figs. 1.a-b show the density and temperature profiles, $\rho_N(x)$ and $T_N(x)$ respectively, measured for $N = 8838$, $\eta = 0.5$ and different gradients ΔT , which are in general nonlinear. Similar profiles are measured for different N , η and ΔT . Unsurprisingly, these profiles exhibit strong finite size effects, see insets in Figs. 1.a-b. Moreover, the thermal walls act as defect lines disrupting the structure of the surrounding fluid, a perturbation that

spreads for a finite penetration length toward the bulk fluid, defining two boundary layers where finite size effects and boundary corrections concentrate and become maximal, see insets in Figs. 1.a-c. In order to minimize spurious boundary corrections, we proceed to eliminate these boundary layers by removing from the profiles the two cells immediately adjacent to each wall (see shaded areas in Fig. 1) [24]. We also measured the reduced pressure $Q_N \equiv \pi \ell^2 P_N$ in each case (with P_N the pressure) by averaging in the bulk the virial pressure profiles, which are constant and agree in all cases with the pressure measured at the walls, finding also strong finite size corrections, see Figs. 1.c-d. Macroscopic LTE implies that, locally, the density and temperature fields should be related via the equilibrium equation of state (EoS), $Q = \rho T \bar{Q}(\rho, T)$, where $\bar{Q}(\rho, T)$ is the compressibility factor [19]. Top panel in Fig. 2 shows results for $\bar{Q}_N \equiv Q_N/[T_N(x)\rho_N(x)]$ measured out of equilibrium, as a function of $\rho_N(x)$ and $T_N(x)$. Note that each nonequilibrium simulation, for fixed $(\Delta T, \eta, N)$, covers a fraction of the EoS surface, thus improving the sampling when compared to equilibrium simulations, which yield a single point on this surface. As hard disks are athermal (i.e. temperature trivially scales out of all thermodynamic relations), the associated \bar{Q} depends exclusively on density, meaning that a complete collapse is expected for the projection of the EoS surface on the $\bar{Q}-\rho$ plane, as we indeed observe, see top panel in Fig. 2. Strikingly, although density and temperature profiles, as well as pressures, all depend strongly on N , see Fig. 1, the measured \bar{Q}_N as a function of the local density exhibits no finite size corrections at all, see bottom panel in Fig. 2 where a total of 2530 data points for different $N \in [1456, 8838]$, $\eta \in [0.05, 0.65]$ and $T_0 \in [2, 20]$ are shown. This strongly suggests a compelling structural decoupling between the bulk fluid, which behaves macroscopically and thus obeys locally the thermodynamic EoS, and the boundary layers near the thermal walls, which sum up all sorts of spurious finite-size and boundary corrections to renormalize the effective boundary conditions on the remaining bulk. This remarkable bulk-boundary decoupling phenomenon, instrumental in the recent discovery of novel scaling laws in nonequilibrium fluids [25], is even more surprising at the light of the long range correlations present in nonequilibrium fluids [4, 17, 18]. For comparison, we include in Fig. 2 (bottom) data from several extensive equilibrium simulations carried with different methods during the last 60 years [20, 26], as well as the Henderson EoS approximation [27], which is reasonably accurate in the fluid phase. The bottom inset in Fig. 2 shows a fine comparison of a running average of our data and the equilibrium simulations in literature, once the leading Henderson behavior has been subtracted. An excellent agreement is found to within 1% relative error, confirming the validity and robustness of macroscopic LTE and the bulk-boundary decoupling phenomenon here reported. The

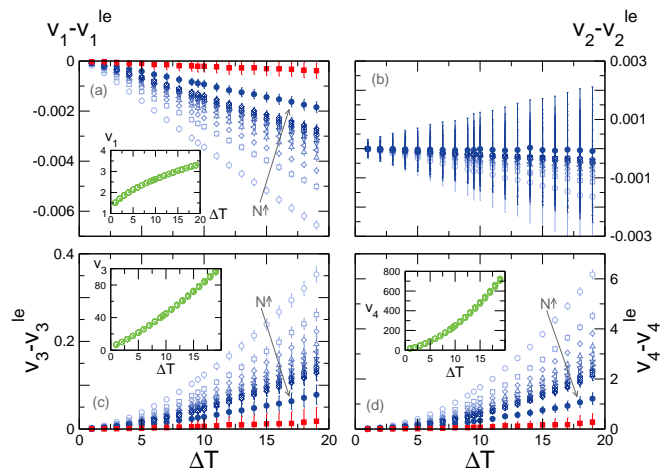


FIG. 3. (Color online) Velocity moments after subtracting the LTE contribution, as a function of ΔT for $\eta = 0.5$ and varying N . Filled symbols correspond to the $N \rightarrow \infty$ limit before (\bullet) and after (\blacksquare) correcting the LTE values for the discretization of hydrodynamic profiles and their fluctuations (see Appendix B). After the correction, no deviations from LTE are observed in velocity moments. The insets show the moments before subtracting the LTE part.

accuracy of our data for the EoS is surprising taking into account that local cells have at most 500 particles, and many fewer in the typical case. Note that our data include points across and beyond the controversial liquid-hexatic-solid phase transition regime [20]. In fact, for $\eta \gtrsim 0.6$ a coexistence between a fluid phase near the hot wall and a solid-like phase near the cold one is established, see middle inset in Fig. 2 where we plot a typical configuration in this nonequilibrium coexistence regime with two color codings, one representing the local angular order parameter ψ_6 [20] which picks the local hexatic order of the symmetry-broken phase (top), and a second color code representing kinetic energy (bottom). This interesting nonequilibrium fluid/solid coexistence will be investigated in detail in a forthcoming paper [29].

The macroscopic notion of LTE that we have just confirmed does not carry over however to microscopic scales. The local statistics associated to a fluid's mNESS must be more complicated than a local Gibbs measure, containing small (but intricate) corrections which are essential for transport to happen [30]. To search for these corrections, we first measured the local velocity statistics (not shown), which turns out to be indistinguishable within our precision from a local Maxwellian distribution with the associated local hydrodynamic fields as parameters. Experience with stochastic lattice gases [12, 16] suggests that deviations from LTE are more easily detected in global observables, so we also measured the global velocity moments $v_n \equiv \langle N^{-1} \sum_{i=1}^N |\mathbf{v}_i|^n \rangle$, with $n = 1, 2, 3, 4$, and compared them with the LTE predictions based on a local Gaussian measure, $v_n^{\text{le}} \equiv \frac{a_n}{\eta} \int_0^1 dx \rho(x) T(x)^{n/2}$ (see Appendix B), with $a_1 = \sqrt{\pi/2}$, $a_2 = 2$, $a_3 = 3\sqrt{\pi/2}$ and

$a_4 = 8$. The LTE corrections we are looking for are tiny, so several correcting factors must be taken into account, e.g. the effect of the discretized hydrodynamic profiles and their fluctuations on v_n^{le} , and the appropriate error propagation, see Appendix B. Fig. 3 shows the first four velocity moments as a function of ΔT , after subtracting the (uncorrected) LTE contribution, as well as the $N \rightarrow \infty$ extrapolation before and after the corrections to v_n^{le} mentioned above. Although a naive comparison of velocity moments with raw LTE estimates would suggest that LTE already breaks down at this level, it becomes apparent that, after properly accounting for all corrections mentioned, no deviations from LTE are observed in velocity moments.

To further pursue the analogy with stochastic lattice gases [12, 16], we also studied the central moments $m_n(u) \equiv \langle (u - \langle u \rangle)^n \rangle$ of the fluid's total energy per particle, $u \equiv N^{-1} \sum_{i=1}^N \frac{1}{2} m \mathbf{v}_i^2$. Figs. 4.a-c show the measured $m_n(u)$, $n = 1, 2, 3$, as a function of ΔT for $\eta = 0.5$ and different N , together with the $N \rightarrow \infty$ extrapolation of our data and the (corrected) LTE estimates for energy moments, $m_n(u)^{\text{le}}$ (see Appendix B). We observe that, while the average energy does indeed follow the LTE behavior, $\langle u \rangle \sim \langle u \rangle^{\text{le}}$, energy fluctuations (as captured by $m_2(u)$ in Fig. 4.b) exhibit increasing deviations from the LTE estimate. In fact, the excess energy fluctuations scale linearly with the squared gradient, $\delta m_2(u) \equiv N[m_2(u) - m_2(u)^{\text{le}}] \approx +\Delta T^2/40$, see Fig. 4.d, a result strongly reminiscent of the behavior observed in schematic models like the Kipnis-Marchioro-Presutti (KMP) model of heat transport or the symmetric exclusion process (SEP) [16], where $\delta m_2(u) = \pm \Delta T^2/12$. Interestingly, energy fluctuations for hard disks are enhanced with respect to LTE, $\delta m_2(u) > 0$, as happens for the KMP model and contrary to the observation for SEP [16], although the excess amplitude is roughly three times smaller for disks. Why do we detect corrections to LTE in energy fluctuations and not for velocity moments? The answer to this natural question lies in the nonlocal character of energy fluctuations. In fact, while v_2 includes only a sum of local factors, $m_2(u)$ includes nonlocal contributions of the form $\langle \mathbf{v}_i^2 \mathbf{v}_j^2 \rangle$, $i \neq j$, summed over the whole system. Small, $\mathcal{O}(N^{-1})$ corrections to LTE extending over large, $\mathcal{O}(N)$ regions give rise to weak long-range correlations in the system which, when summed over macroscopic regions, yield a net contribution to energy fluctuations, which thus depart from the LTE expectation [4, 5, 16]. In this way, the observed breakdown of LTE at the energy fluctuation level is a reflection of the nonlocality of the underlying large deviation function governing fluctuations in the nonequilibrium fluid. This result is, to our knowledge, the first evidence of a nonlocal LDF in a realistic model fluid, and suggests to study in more detail large deviation statistics in hard disks. A first step in this direction consists in investigating the statis-

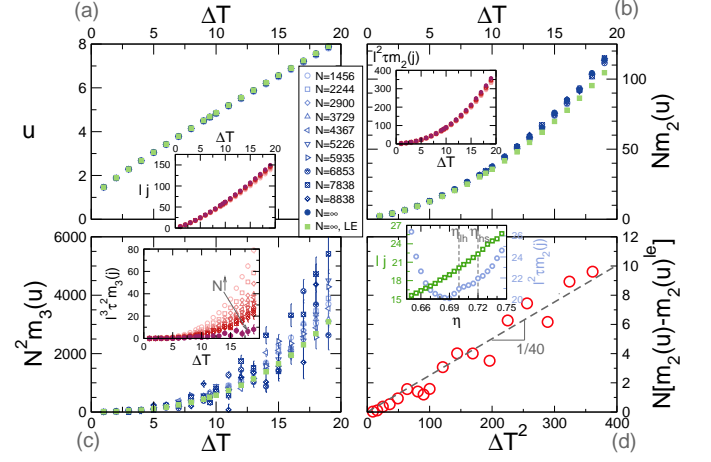


FIG. 4. (Color online) (a), (b) and (c): Scaled central moments of the total energy as a function of ΔT for $\eta = 0.5$ and varying N . Filled symbols correspond to the $N \rightarrow \infty$ limit of our data (\bullet) and after assuming LTE (\blacksquare). The insets show the scaled central moments of the time-averaged current vs ΔT for $\eta = 0.5$ and varying N . (d) The excess energy variance (as compared to LTE) scales linearly with ΔT^2 with a slope $\approx 1/40$. Inset: Average current and its variance as a function of the global packing fraction. The liquid-to-hexatic (η_{lh}) and hexatic-to-solid (η_{hs}) transition points are signaled.

tics of the energy current flowing through the system during a long time τ , a key observable out of equilibrium. In order to do so, and given the difficulties in sampling the tails of an LDF, we measured the central moments of the time-integrated energy current for $\tau = 10$, see insets in Fig. 4. In particular, our measurements for the current third moment seem compatible with zero $\forall \Delta T$ in the asymptotic $N \rightarrow \infty$ limit, suggesting Gaussian current fluctuations within our accuracy level. Interestingly, while the average current (as well as the total energy moments) are smooth functions of the global packing fraction, current fluctuations exhibit a remarkable structure, see inset in Fig. 4.d, with a minimum right before the liquid-to-hexatic equilibrium transition $\eta_{\text{lh}} \approx 0.7$, where a first inflection point appears, followed by another one at the hexatic-to-solid transition $\eta_{\text{hs}} \approx 0.72$, showing that hints of the double phase transition arise in the transport properties of the nonequilibrium hard-disks fluid.

In summary, we have probed LTE in a quintessential model fluid, the hard-disks system, finding that macroscopic LTE is a very robust property. This is so even under strong finite-size effects, due to a remarkable bulk-boundary structural decoupling by which all sorts of finite-size and boundary corrections are renormalized into new boundary conditions for the bulk fluid, which in turn obeys the macroscopic laws. We use these properties to measure with high accuracy the hard-disks EoS, even across the fluid-hexatic-solid transition regime. However, weak but clear violations of microscopic or statistical LTE are found in the fluctuations of the total energy which strongly suggest that the nonequilibrium potential

governing the driven fluid's macroscopic behavior is intrinsically non-local. It would be therefore interesting to investigate more in depth the large deviation statistics of hard disks, using both macroscopic fluctuation theory and simulations of rare events.

Financial support from Spanish MICINN project FIS2009-08451, NSF Grant DMR1104500, University of Granada, Junta de Andalucía projects P06-FQM1505, P09-FQM4682 and GENIL PYR-2014-13 project is acknowledged.

* jpozo@onsager.ugr.es

† garrido@onsager.ugr.es

‡ phurtado@onsager.ugr.es

- [1] J.L. Lebowitz, *Nonequilibrium statistical physics today: Where shall we go from here?*, AIP Conf. Proc. **1332**, 3 (2011).
- [2] G. Gallavotti, *Nonequilibrium and Irreversibility*, Springer, Berlin (2014).
- [3] F. Bonetto, J.L. Lebowitz, and L. Rey-Bellet, *Fourier's law: a challenge to theorists*, in *Mathematical Physics 2000*, A. Fokas et al (eds.), Imperial College Press, London (2000), pp. 128-150.
- [4] L. Bertini, A. De Sole, D. Gabrielli, G. Jona-Lasinio and C. Landim, Phys. Rev. Lett. **87**, 040601 (2001); J. Stat. Phys. **107**, 635 (2002); Phys. Rev. Lett. **94**, 030601 (2005); J. Stat. Phys. **123**, 237 (2006); J. Stat. Mech. P07014 (2007); J. Stat. Phys. **135**, 857 (2009); arXiv:1404.6466.
- [5] T. Bodineau and B. Derrida, Phys. Rev. Lett. **92**, 180601 (2004); Phys. Rev. E **72**, 066110 (2005); B. Derrida, J. Stat. Mech. P07023 (2007).
- [6] P.I. Hurtado and P.L. Garrido, Phys. Rev. Lett. **102**, 250601 (2009); J. Stat. Mech. P02032 (2009); Phys. Rev. E **81**, 041102 (2010); Phys. Rev. Lett. **107**, 180601 (2011); P.I. Hurtado, C.P. Espigares, J.J. del Pozo and P.L. Garrido, J. Stat. Phys. **154**, 214 (2014); C.P. Espigares, P.L. Garrido, and P.I. Hurtado, Phys. Rev. E **87**, 032115 (2013).
- [7] P.I. Hurtado, C.P. Espigares, J.J. del Pozo and P.L. Garrido, Proc. Natl. Acad. Sci. USA **108**, 7704 (2011).
- [8] D. Evans and G. Morriss, *Statistical Mechanics of Nonequilibrium Liquids*, Cambridge University Press, Cambridge (2008).
- [9] J.L. Lebowitz, Physica (Amsterdam) **194A**, 1 (1993). [6] N.I. Chernov, G.L. Eyink, J.L. Lebowitz, and Ya.G. Sinai, Phys. Rev. Lett. **70**, 2209 (1993); Commun. Math. Phys. **154**, 569 (1993). G. Gallavotti, J. Stat. Phys. **78**, 1571 (1995).
- [10] G. Gallavotti and E.G.D. Cohen, Phys. Rev. Lett. **74**, 2694 (1995); J. Stat. Phys. **80**, 931 (1995); G. Gallavotti, J. Stat. Phys. **84**, 899 (1996).
- [11] N.I. Chernov and J.L. Lebowitz, Phys. Rev. Lett. **75**, 2831 (1995); J. Stat. Phys. **86**, 953 (1997).
- [12] H. Spohn, *Large Scale Dynamics of Interacting Particles*, Springer-Verlag, Berlin (1991).
- [13] L.D. Landau and E.M. Lifshitz, *Fluid Mechanics*, 2nd ed., Pergamon Press, Oxford (1987).
- [14] S.R. de Groot and P. Mazur, *Non-Equilibrium Thermodynamics*, Dover Publications (2011).
- [15] H. Touchette, Phys. Rep. **478**, 1 (2009)
- [16] B. Derrida, J.L. Lebowitz, and E.R. Speer, Phys. Rev. Lett. **87**, 150601 (2001); J. Stat. Phys. **107**, 599 (2002); J. Stat. Phys. **110**, 775 (2003); L. Bertini, D. Gabrielli, and J.L. Lebowitz, J. Stat. Phys. **121**, 843 (2005).
- [17] J.M. Ortiz de Zárate and J.V. Sengers, *Hydrodynamic Fluctuations in Fluids and Fluid Mixtures*, Elsevier, Amsterdam (2006).
- [18] P.L. Garrido, J.L. Lebowitz, C. Maes and H. Spohn, Phys. Rev. A **42**, 1954 (1990).
- [19] *Theory and simulation of hard-sphere fluids and related systems*, A. Mulero (ed.), Springer, Heidelberg (2008).
- [20] E.P. Bernard and W. Krauth, Phys. Rev. Lett. **107**, 155704 (2011); M. Engel, J.A. Anderson, S.C. Glotzer, M. Isobe, E.P. Bernard, and W. Krauth, Phys. Rev. E **87**, 042134 (2013).
- [21] S. Lepri, R. Livi, and A. Politi, Phys. Rep. **377**, 1 (2003); A. Dhar, Adv. Phys. **57**, 457 (2008).
- [22] J.-P. Eckmann and L.-S. Young, Europhys. Lett. **68**, 790 (2004).
- [23] Note that the fitted exponent α exhibits a pronounced dependence on N and ΔT , with $\alpha \in [0.681, 0.715]$ and no coherent asymptotic behavior, another trait of finite size corrections.
- [24] A. Tenenbaum, G. Ciccotti, and R. Gallico, Phys. Rev. A **25**, 2778 (1982).
- [25] J.J. del Pozo, P.L. Garrido and P.I. Hurtado, arXiv:1401.5244.
- [26] N. Metropolis, A.W. Rosenbluth, M.N. Rosenbluth, A.H. Teller, and E. Teller, J. Chem. Phys. **21**, 1087 (1953); B.J. Alder, J. Chem. Phys. **49**, 3688 (1968); J.J. Erpenbeck and M. Luban, Phys. Rev. A **32**, 2920 (1985); C.H. Mak, Phys. Rev. E **73**, 065104 (2006); J. Kolafa and M. Rottner, Mol. Phys. **104**, 3435 (2006);
- [27] The Henderson EoS [19, 28] can be written as
$$\bar{Q}_{H77}(\rho) = \left[\frac{1 + \rho^2/8}{(1 - \rho)^2} - 0.043 \frac{\rho^4}{(1 - \rho)^3} \right]$$
- [28] D. Henderson, Mol. Phys. **34**, 301 (1977).
- [29] J.J. del Pozo, P.L. Garrido and P.I. Hurtado, in preparation.
- [30] Note that the local Gibbs measure in a fluid is even in velocities, while for instance the local energy current is odd, thus leading to a zero average energy current for a mLTE state, in contradiction with observed behavior. It is therefore the tiny corrections to mLTE that are responsible for transport.

APPENDIX A

Corrections due to discretization effects in density and temperature profiles

We measure in the steady state the local temperature (i.e. local average kinetic energy) and local packing fraction at each of the 15 cells in which we divide the simulation box along the gradient (i.e. x -) direction. In order to minimize cells boundary effects, when a disk overlaps with any of the imaginary lines separating two neighboring cells, it contributes to the density and kinetic energy of each cell proportionally to its overlapping area. Note that the number of cells is constant in all simulations, independently of N , η , T_0 or T_L , so each cell becomes *macroscopic* asymptotically as $N \rightarrow \infty$. We now relate averages around a finite neighborhood of a given point in space with the underlying continuous profiles in order to subtract any possible bias or systematic correction from the data. In particular, let's T_C and ρ_C be the temperature and packing fraction in a cell centered at $x_c \in [0, L]$ of size Δ . Assuming that there exist continuous (hydrodynamic) profiles $T(x)$ and $\rho(x)$, we can relate the cell averages to the continuous profiles by noting that

$$T_C = \frac{1}{\Delta \rho_C} \int_{x_c - \Delta/2}^{x_c + \Delta/2} dx \rho(x) T(x),$$

$$\rho_C = \frac{1}{\Delta} \int_{x_c - \Delta/2}^{x_c + \Delta/2} dx \rho(x).$$

We may expand now the continuous profiles around x_c inside the cell of interest and solve the above integrals. Keeping results up to Δ^2 order we arrive at

$$T_C = \frac{1}{\rho_C} \left[\rho(x_c) T(x_c) + \frac{\Delta^2}{24} \frac{d^2}{dx^2} [\rho(x) T(x)]_{x=x_c} + O(\Delta^3) \right],$$

$$\rho_C = \rho(x_c) + \frac{\Delta^2}{24} \frac{d^2 \rho(x)}{dx^2} \Big|_{x=x_c} + O(\Delta^3).$$

By inverting the above expressions, we obtain the desired result, namely

$$T(x_c) = T_C - \frac{1}{24} \left[\frac{2}{\rho_C} (\rho_{C+1} - \rho_C) (T_{C+1} - T_C) + T_{C+1} - 2T_C + T_{C-1} \right], \quad (1)$$

$$\rho(x_c) = \rho_C - \frac{1}{24} [\rho_{C+1} - 2\rho_C + \rho_{C-1}], \quad (2)$$

which yields the points of the underlying continuous profiles, $T(x_c)$ and $\rho(x_c)$, in terms of the measured observables, T_C and ρ_C respectively. These corrections to the cell density and temperature are typically small ($\sim 0.1\%$), though important to disentangle the different finite-size effects in order to obtain the striking collapse of the hard-disks EoS described in the main text.

APPENDIX B

Velocity moments under local equilibrium and corrections

The local equilibrium probability measure to observe a particle configuration with positions \mathbf{r}_i and momenta \mathbf{p}_i , $\forall i \in [1, N]$, can be written as

$$\mu^{\text{le}}(\mathbf{r}_1, \dots, \mathbf{r}_N; \mathbf{p}_1, \dots, \mathbf{p}_N) \propto \exp \left\{ - \sum_{i=1}^N \beta(\epsilon x_i) \left[\frac{\mathbf{p}_i^2}{2m} + \frac{1}{2} \sum_{j \neq i} \Phi(\mathbf{r}_i - \mathbf{r}_j) \right] \right\}, \quad (3)$$

where ϵ is the parameter that connects the microscopic scale with the hydrodynamic one, $\beta(\epsilon x_i)$ is the local inverse temperature around x_i , and $\Phi(\mathbf{r})$ is the interparticle potential. Note that we have already assumed that temperature varies only along the x -direction. Under this microscopic LTE hypothesis, one may argue that the probability density for any particle to have a velocity modulus equal to v is given by

$$f(v) = \frac{v}{\eta} \int_0^1 dx \frac{\rho(x)}{T(x)} \exp \left[- \frac{v^2}{2T(x)} \right], \quad (4)$$

with $\eta = \int_0^1 dx \rho(x)$ the global packing fraction. Then, by definition, the local equilibrium velocity moments follow as

$$v_n^{\text{le}} \equiv \langle v^n \rangle_{\text{le}} = \frac{a_n}{\eta} \int_0^1 dx \rho(x) T(x)^{n/2} \quad (5)$$

where $a_1 = (\pi/2)^{1/2}$, $a_2 = 2$, $a_3 = 3(\pi/2)^{1/2}$ and $a_4 = 8$. Now, in order to compare the measured velocity moments in the main text with the local equilibrium expectations, v_n^{le} , we first have to express the latter in terms of our observables. For that, three steps should be taken, namely:

- Write eq. (5) as a function of the measured cell temperatures and densities, T_C and ρ_C , following eqs. (1)-(2).
- Take into account the fact that both T_C and ρ_C have errorbars and thus should be considered as fluctuating variables around their average. Note also that the fluctuations of $\rho(x)$ should be constrained to a constant average η .
- Consider the correct error propagation to compute the errorbars of v_n^{le} .

B.1 Conversion to cell variables

We now express eq. (5) in terms of cell variables. In order to proceed, we write

$$\tilde{v}_n^{\text{le}} = \frac{a_n}{\eta} \sum_C \int_{x_c - \Delta/2}^{x_c + \Delta/2} dx \rho(x) T(x)^{n/2} \quad (6)$$

where x_c are the center of the cells. We may expand the previous expression up to order Δ^2 to arrive at

$$\begin{aligned} \tilde{v}_n^{\text{le}} = \frac{a_n}{\eta} \Delta \sum_C \left[\rho(x_c) T(x_c)^{n/2} + \frac{\Delta^2}{24} \left[\frac{d^2 \rho(x)}{dx^2} \Big|_{x=x_c} T(x_c)^{n/2} + n \frac{d\rho(x)}{dx} \Big|_{x=x_c} T(x_c)^{n/2-1} \frac{dT(x)}{dx} \Big|_{x=x_c} \right. \right. \\ \left. \left. + \frac{n}{2} \left(\frac{n}{2} - 1 \right) \rho(x_c) T(x_c)^{n/2-2} \left(\frac{dT(x)}{dx} \Big|_{x=x_c} \right)^2 + \frac{n}{2} \rho(x_c) T(x_c)^{n/2-1} \frac{d^2 T(x)}{dx^2} \Big|_{x=x_c} \right] \right], \end{aligned} \quad (7)$$

and using eqs. (1)-(2), we obtain

$$\tilde{v}_n^{\text{le}} = \frac{\Delta a_n}{\eta} \sum_C \rho_C T_C^{n/2} + \frac{\Delta a_n}{96\eta} n(n-2) \sum_C \rho_C T_C^{n/2-2} (T_{C+1} - T_C)^2 \quad (8)$$

B.2 Accounting for cell temperature and density fluctuations

Due to the finite number of measurements in simulations, any magnitude and, in particular, the cell observables will exhibit fluctuations that will affect the observed averaged behavior. We now assume that these fluctuations are gaussian and obey

$$\begin{aligned} \rho_C = \bar{\rho}_C + \gamma_C \xi_C, \quad \text{Prob}(\xi_1, \dots, \xi_M) = \sqrt{2\pi M} \prod_{i=1}^M \left[\frac{1}{\sqrt{2\pi}} e^{-\xi_i^2/2} \right] \delta \left(\sum_{i=1}^M \xi_i \right) \\ T_C = \bar{T}_C + \sigma_C \zeta_C, \quad \text{Prob}(\zeta_1, \dots, \zeta_M) = \prod_{i=1}^M \left[\frac{1}{\sqrt{2\pi}} e^{-\zeta_i^2/2} \right] \end{aligned} \quad (9)$$

where $M = 15$ is the number of cells, γ_C and σ_C are the measured (empirical) errors associated to the average density and temperature at cell C , $\bar{\rho}_C$ and \bar{T}_C respectively, and ξ_C and ζ_C are gaussian random variables with zero mean and variance one. Notice that the density noise takes into account the fact that the total density is constant. For the case studied here we may assume that the errors are $\mathcal{O}(\Delta)$ and we will expand results up to orders σ^2 or γ^2 . Now, by substituting ρ_C and T_C in eq. (8) by the fluctuating expressions in (9) and then averaging over the noise distributions, we arrive at

$$v_n^{\text{le}} \equiv \langle \tilde{v}_n^{\text{le}} \rangle_{\xi, \zeta} = \frac{\Delta a_n}{\eta} \sum_C \bar{\rho}_C \langle T_C^{n/2} \rangle_{\zeta} + \frac{\Delta a_n}{96\eta} n(n-2) \sum_C \bar{\rho}_C \bar{T}_C^{n/2-2} (\bar{T}_{C+1} - \bar{T}_C)^2 + \mathcal{O}(\Delta^3) \quad (10)$$

where

$$\langle T_C^{n/2} \rangle_\zeta = \bar{T}_C^{n/2} + \frac{1}{8}n(n-2)\bar{T}_C^{n/2-2}\sigma_C^2 + O(\sigma_C^4) \quad (11)$$

It therefore becomes clear that fluctuations in each cell add a small correction to v_n^{le} .

B.3 Computing errorbars in the local equilibrium approximation

Once we know how to compute v_n^{le} from our set of data, we want to obtain their errorbars, χ_n , defined as

$$\chi_n^2 = \langle (\tilde{v}_n^{\text{le}})^2 \rangle_{\xi, \zeta} - \langle \tilde{v}_n^{\text{le}} \rangle_{\xi, \zeta}^2 \quad (12)$$

In order to do so, we first need to know that

$$\langle \xi_C^2 \rangle_\xi = 1 - \frac{1}{M} \quad , \quad \langle \xi_C \xi_{C'} \rangle_\xi = -\frac{1}{M} \quad \text{if } C \neq C' . \quad (13)$$

It is then easy to show that

$$\chi_n^2 = \left(\frac{\Delta a_n}{\eta} \right)^2 \left[\sum_C (b_n \sigma_C^2 \bar{\rho}_C^2 \bar{T}_C^{n-2} + \gamma_C^2 \bar{T}_C^n) - \frac{1}{M} \left(\sum_C \gamma_C \bar{T}_C^{n/2} \right)^2 \right] \quad (14)$$

with $b_1 = 1/4$, $b_2 = 1$, $b_3 = 9/4$ and $b_4 = 4$. To better appreciate the relevance of the above corrections, it is useful to define

$$(v_n^{\text{le}})_0 \equiv \frac{\Delta a_n}{\eta} \sum_C \bar{\rho}_C \bar{T}_C^{n/2} \quad , \quad (v_n^{\text{le}})_{\text{corr}} \equiv v_n^{\text{le}} - (v_n^{\text{le}})_0 \quad (15)$$

That is, $(v_n^{\text{le}})_{\text{corr}}$ contains the Δ^2 effects due to the finite sizes of the boxes and the effects of the errors on the measured temperature and density profiles. Though small, this correction term is essential to confirm that corrections to LTE does not show up in our measurements of velocity moments, see main text.